Contribution of thermally scattered electrons to atomic resolution elemental maps

B. D. Forbes,[1] A. J. D'Alfonso,[1] R. E. A. Williams,[2] R. Srinivasan,[2] H. L. Fraser,[2] D. W. McComb,[2] B. Freitag,[3] D. O. Klenov,[3] and L. J. Allen[1,*]

[1]*School of Physics, University of Melbourne, Parkville, Victoria 3010, Australia*

[2]*Department of Materials Science and Engineering, The Ohio State University, 477 Watts Hall, 2041 College Road, Columbus, Ohio 43210, USA*

[3]*FEI Company, Building AAE, Achtseweg Noord 5, Eindhoven, The Netherlands*

(Received 9 May 2012; published 18 July 2012)

Electron energy-loss spectroscopy (EELS) and energy dispersive x-ray (EDX) analysis in scanning transmission electron microscopy (STEM) have the ability to produce elemental maps of a specimen at atomic resolution. In this paper we present EELS and EDX maps for the oxygen K shell in ⟨001⟩ strontium titanate. The results initially seem to be anomalous since substantially more signal is obtained when the STEM probe is above the columns containing both titanium and oxygen than when it is above those containing only oxygen. This is at variance with the stoichiometry: the density of oxygen in both types of columns is the same. Using theory, we show that an understanding of the direct contribution to the recorded signal from electrons which have been thermally scattered is the key to understanding these results. We contrast these results with elemental maps of ⟨110⟩ strontium titanate. While the experimental results are not directly interpretable, they are in concert with simulations from first principles such as those presented in this paper.

DOI: 10.1103/PhysRevB.86.024108 PACS number(s): 61.05.jd

I. INTRODUCTION

Elemental mapping in two dimensions at atomic resolution using core-loss electron energy-loss spectroscopy (EELS) has been under development since 2007[1–4] and is now at the point where it can be used to solve problems of technological interest.[5] As an alternative to EELS one can use energy-dispersive x-ray (EDX) analysis, detecting the x rays which are emitted subsequent to ionization. EDX elemental mapping is an incoherent mode of imaging, as is the widely used technique of *Z*-contrast imaging, but with the advantage that elemental information is directly available for a range of different elements and x-ray peaks. An advantage of EDX mapping relative to EELS is the accessibility of higher energy-loss peaks and their associated increased localization. The first two-dimensional atomic resolution elemental maps based on EDX were published as recently as 2010[6,7] and considerable improvements in the quality of such data have followed.[8]

Atomic resolution maps obtained in EELS are based on detecting electrons that have lost energy on transiting through the specimen due to inelastic scattering and that are scattered into a range of angles in the forward direction, defined by the collection aperture of the spectrometer. We then consider the integrated signal from a subset of those electrons falling into a suitable energy-loss window above the threshold energy for a particular core-loss edge. When detecting x rays associated with a particular edge in the EDX imaging mode, all possible kinematics of the inelastically scattered fast electron are effectively sampled since there is no restriction to scattering in the forward direction imposed by the EELS spectrometer. In addition, the energy window effectively extends over all possible energies above the threshold. So we expect that EELS with a large detector aperture and a large energy window, starting at threshold, would have underlying physics similar to those of EDX-based elemental mapping.

The similarity in the underlying physics for EDX and EELS mapping is borne out by the results we discuss in Sec. II. Apparently anomalous behavior is seen in both EELS and EDX elemental maps for the oxygen K-shell signal in ⟨001⟩ strontium titanate: substantially more signal is obtained when the scanning transmission electron microscopy (STEM) probe is above columns containing both titanium and oxygen compared to columns containing only oxygen, despite the density of oxygen in both types of columns being the same (one atom per 3.905 Å). Precisely this effect has also been noted in previous work by Dudeck and coworkers.[9]

II. EXPERIMENTAL DATA

EELS data were obtained at Ohio State University. Figure 1 shows a line scan taken across successive Ti/O and O columns which shows the substantially enhanced signal on the Ti/O columns compared with that on the O columns. Data were collected at an accelerating voltage of 300 kV on an aberration-corrected FEI Titan with a probe-forming convergence semiangle of approximately 17 mrad and a collection semiangle at the detector of 35 mrad. An energy window of 40 eV above the edge onset was used. The thickness of the specimen was estimated to be 200 Å.

Elemental mapping using EDX was also performed on ⟨001⟩ strontium titanate at FEI Company in Eindhoven. An aberration-corrected Titan G2 microscope equipped with a Super-X detector[8] was used. The accelerating voltage was 200 kV and the probe-forming convergence semiangle was approximately 23 mrad. The specimen thickness in this case was somewhat greater, approximately 700 Å. The same apparently anomalous behavior seen in EELS was noted when detecting x rays associated with the K-shell edge. A map for a single two-dimensional scan based on the oxygen K edge (raw data) is shown in Fig. 2(a), whereas a filtered average using a 5 × 5-pixel moving-average square window is shown in Fig. 2(b). A substantial enhancement of the signal on the Ti/O columns relative to the pure O columns is, once again, evident.

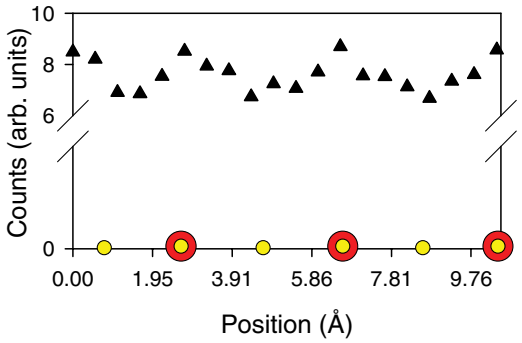

FIG. 1. (Color online) An EELS line scan from ⟨001⟩ strontium titanate monitoring the oxygen K-shell signal along successive Ti/O and pure O columns. Experimental conditions are detailed in the text. The density of oxygen in both types of columns is the same in this projection. Nevertheless, there is a marked and consistent disparity in the signals. The positions of the Ti/O [large (red) rings and small, inset (yellow) circles] and O [small (yellow) circles] columns are indicated.

Considering thermal diffuse scattering, which is expected to redistribute the electron flux away from the column, one might initially argue that, for both the EELS and the EDX cases, a lower signal should be obtained when the probe is on the Ti/O columns than when it is on the O columns. This view seems reasonable on the basis of previously reported EELS elemental maps, where it was shown that thermal diffuse scattering can reduce the signal from a column relative to off-column probe positions, explained by the depletion of the elastically scattered probe on the column by thermal scattering.[1,10] However the data in Figs. 1 and 2 clearly show that, in this case, the opposite is true. This is consistent with the results of a coeval study by Dudeck *et al.*,[9] who observed that EELS maps of oxygen in strontium titanate did not appear to reflect the stoichiometry but offered no explanation for the observation.

We show that the contribution to the signal from thermally scattered electrons (those which have already excited a phonon, perhaps multiple times) is key to understanding the enhancement of the signal seen in the experimental data

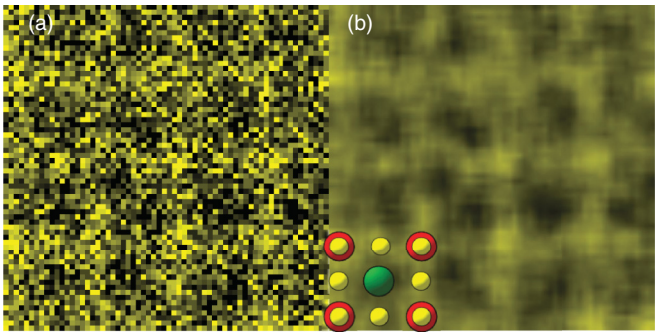

FIG. 2. (Color online) (a) An EDX elemental map of ⟨001⟩ strontium titanate monitoring the oxygen K_α line for a single scan (raw data). Experimental conditions are given in the text. (b) The result of applying a 5 × 5-pixel moving-average square window to the original data is shown. The projected structure is indicated. The positions of Ti/O columns are indicated by the large (red) rings and smaller, inset (yellow) circles; those of O columns, by small yellow circles; and that of an Sr column, by the large, filled (green) circle.

when the probe is on the column containing the heavier Ti atoms. This is due to ionization by the thermally scattered electrons of oxygen atoms surrounding the column (and quite far from it in some cases). This insight is made possible by using the recently introduced model for thermal scattering, which employs a Born-Oppenheimer (BO) approximation to solve the quantum mechanical many-body problem.[11] This model allows one to track the contribution to the measured signal from both elastically and thermally scattered electrons separately, unlike the widely used frozen phonon model for thermal scattering.[12,13] It is precisely the ability to consider each of these contributions that throws light on the crucial role of the thermally scattered electrons.

III. THEORY

In the BO approximation model[11] the cross section for ionization as a function of probe position is obtained by a suitably weighted averaging of contributions from the many possible configurations of the crystal seen by a *single* incident electron. The fraction of the incident electrons which undergo inelastic scattering due to ionization can be expressed in the form[11,14–16]

$$I(\mathbf{R},t) = \frac{1}{A^2}\sum_{j=1}^{J}\int_0^t\int_A\int_A \phi_j^*(\mathbf{R},\mathbf{r}_\perp,z) \times W(\mathbf{r}_\perp,\mathbf{r}'_\perp)\phi_j(\mathbf{R},\mathbf{r}'_\perp,z)d\mathbf{r}_\perp d\mathbf{r}'_\perp dz. \quad (1)$$

The position of the STEM probe is denoted by $\mathbf{R}$, t is the thickness of the specimen (along z), A is the area of the unit cell, j labels a particular configuration of the atoms in the crystal, and J denotes the number of different configurations used. The probe function associated with the configuration j at a depth z is given by $\phi_j(\mathbf{R},\mathbf{r}_\perp,z)$, where the coordinate $\mathbf{r}_\perp$ is in the plane perpendicular to the z direction. In general, the effective potential $W(\mathbf{r}_\perp,\mathbf{r}'_\perp)$ for inelastic scattering, in this case due to ionization, is nonlocal, since it depends on the two coordinates $\mathbf{r}_\perp$ and $\mathbf{r}'_\perp$. The signal also depends on the probe function at both $\mathbf{r}_\perp$ and $\mathbf{r}'_\perp$. This means that the relative phase of the probe function at points $\mathbf{r}_\perp$ and $\mathbf{r}'_\perp$ is relevant.

The projected nonlocal potential $W(\mathbf{r}_\perp,\mathbf{r}'_\perp)$ has the form

$$W(\mathbf{r}_\perp,\mathbf{r}'_\perp) = \frac{2\pi m}{h^2 t}\sum_\alpha\sum_{n\neq 0} k_n H^*_{\alpha,n0}(\mathbf{r}_\perp)H_{\alpha,n0}(\mathbf{r}'_\perp) \times \int e^{2\pi i\mathbf{K}'_\perp\cdot(\mathbf{r}_\perp-\mathbf{r}'_\perp)}\delta(k_n - K')d\Omega_{K'}dK', \quad (2)$$

where m is the relativistically corrected electron mass. We have defined the projected transition potential matrix element as

$$H_{\alpha,n0}(\mathbf{r}_\perp) \equiv \int_0^t H_{\alpha,n0}(\mathbf{r})e^{2\pi i(K-K')z}dz. \quad (3)$$

The modulus squared of the transition potential, $|H_{\alpha,n0}|^2$, gives the probability of inelastic scattering from atom α, where ionization occurs from an initial state 0 via the interaction Hamiltonian to a final state n (with wave number k_n for the inelastically scattered electron). The wave number of the incident electron is K (corrected for refraction). The integration over $d\Omega_{K'}$ effectively integrates over all scattered

electrons with wave vector $\mathbf{K}' = (\mathbf{K}'_\perp, K'_z)$ that are pertinent to the experiment subject to the requirement that the magnitude of $\mathbf{K}'$ is constrained by conservation of energy to be on the energy shell defined by $K' = k_n$. In Eq. (3) it has been assumed that $K'_z \approx K'$ (a good approximation for scattering which is predominantly in the forward direction). The range of integration over $d\Omega_{K'}$ is determined by the acceptance angle of the detector in EELS and is the whole solid angle for an EDX experiment. For a detector with a large acceptance angle (and therefore always in the EDX case) the effective potential for inelastic scattering becomes local and Eq. (1) reduces to

$$I(\mathbf{R},t) = \frac{1}{A^2}\sum_{j=1}^{J}\int_0^t\int_A |\phi_j(\mathbf{R},\mathbf{r}_\perp,z)|^2 V(\mathbf{r}_\perp)d\mathbf{r}_\perp dz, \qquad (4)$$

where $V(\mathbf{r}_\perp)$ is now a local ionization potential which can be explicitly written as

$$V(\mathbf{r}_\perp) = \frac{\pi m}{h^2 t}\sum_{n\neq 0}\frac{1}{k_n}\sum_{\alpha}|H_{\alpha,n0}(\mathbf{r}_\perp)|^2. \qquad (5)$$

The propagation of the probe function along z can be calculated using the multislice formulation.[14] We emphasize again that Eq. (4) is the total fraction of the incident electrons that undergo inelastic scattering due to ionization, *including* electrons that have already been thermally scattered.

To separate out the contribution to the signal from electrons which have only been elastically scattered prior to ionization, it is important to realize that the wave function $\psi_0(\mathbf{R},\mathbf{r}_\perp,z)$ for the *elastic* scattering of the probe at depth z can be obtained by a coherent summation of the auxilliary functions $\phi_j(\mathbf{R},\mathbf{r}_\perp,z)$.[11] We note that it has been shown[11] that essentially the same result for $\psi_0(\mathbf{R},\mathbf{r}_\perp,z)$ can be rapidly obtained using the absorptive model of Hall and Hirsch.[17] Consequently the distribution of elastically and thermally scattered electrons can be visualized. Then for the local potential case (a similar approach applies to the more general nonlocal case), the contribution to the total signal from electrons which have been elastically scattered prior to ionization is

$$I_0(\mathbf{R},t) = \frac{1}{A^2}\int_0^t\int_A |\psi_0(\mathbf{R},\mathbf{r}_\perp,z)|^2 V(\mathbf{r}_\perp)d\mathbf{r}_\perp dz. \qquad (6)$$

Consequently, we are also able to calculate the contribution to the total EELS or EDX signal from electrons which have previously been thermally scattered.

As discussed in Sec. I, in the first instance an EDX signal is assumed to be proportional to an EELS signal where the detector is effectively the full solid angle and the energy window encompasses all possible energy losses above the ionization threshold. The fluorescence yields, absorption of x rays by the specimen,[18] and detector efficiency could also be considered but those refinements are not taken into account in this paper.

IV. SIMULATIONS AND DISCUSSION

Figure 3 shows simulated EELS and EDX elemental maps of the oxygen K-shell edge in ⟨001⟩ strontium titanate for the experimental results shown in Figs. 1 and 2, with the simulation

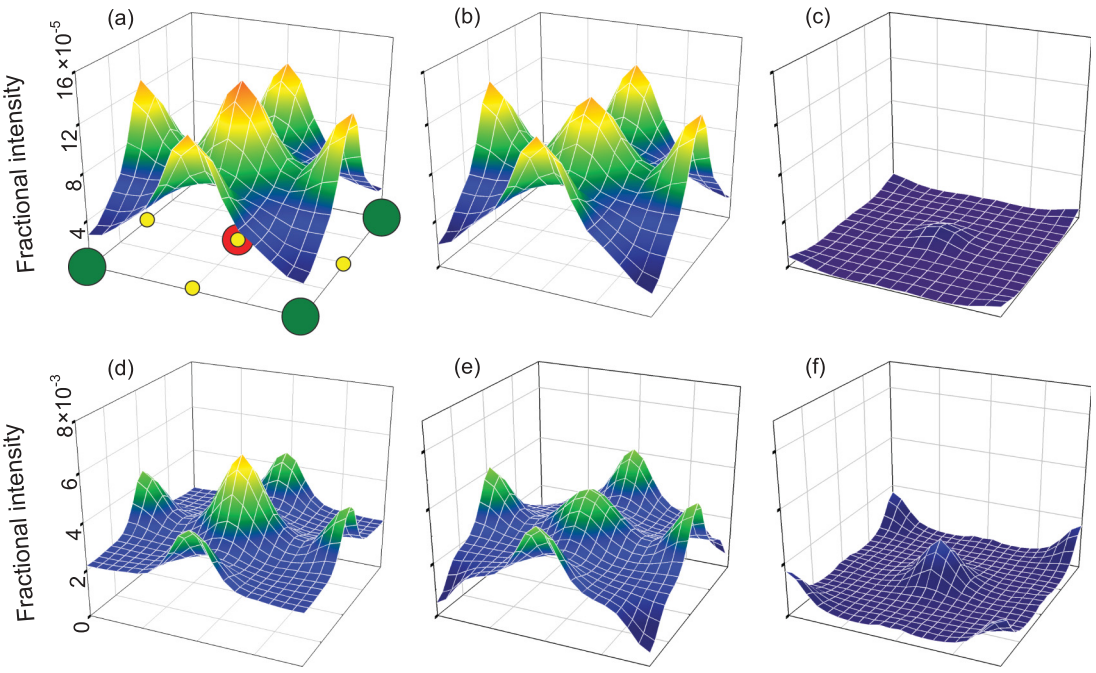

FIG. 3. (Color online) Simulated elemental maps of the signal in the oxygen K edge in ⟨001⟩ strontium titanate across a unit cell. (a)–(c) EELS results for the same imaging conditions pertinent to Fig. 1 (as specified in the text in Sec. II). (a) The total signal, (b) the signal for ionization by elastically scattered electrons, and (c) that due to electrons which were first thermally scattered. (d)–(f) Calculations for the EDX case, with the microscope parameters chosen, as detailed in Sec. II, to correspond with the experimental data in Fig. 2. (d) The total signal, (e) that due to elastically scattered electrons, and (f) that due to ionization by thermally scattered electrons. The projected structure is indicated in (a), with the position of the Ti/O column indicated by the partially visible (red) ring with inset (yellow) circle; visible O columns, by small (yellow) circles; and Sr columns, by large (green) circles.

parameters in each case being those given in Sec. II. These results are separated into contributions from elastically and thermally scattered electrons, as discussed in Sec. III. At the thicknesses used for these calculations (200 Å for EELS and 700 Å for EDX), the total signal is higher on the titanium-oxygen (Ti/O) columns than on the pure oxygen (O) columns. This is reversed if one only calculates the contribution to the signal from electrons which have only scattered elastically (albeit not by a large amount). It is the contribution to the signal from electrons which have been thermally scattered prior to ionizing an atom that ensures that the total signal on the Ti/O columns is significantly greater than that on the pure O columns. The fractional intensity for the EDX results in Fig. 3 can be interpreted as an upper bound since, as already pointed out, fluorescence yields and x-ray absorption in the specimen have not been taken into account.

We now investigate how the signals on the Ti/O and the O columns compare as a function of thickness. In Fig. 4 we have plotted the ratio of the total signal when the probe is on the Ti/O columns to that on the pure O columns as a function of thickness. The parameters specified in Sec. II were used to calculate the EELS result in Fig. 4(a) and the EDX result in Fig. 4(b). The ratio is also shown for the contribution from elastically scattered electrons only. It is shown that the ratio of the full contribution is generally not unity, as one would initially anticipate based on stoichiometry. In the EELS case this ratio can be greater than or less than unity depending on the thickness of the specimen. For the EDX case the ratio is always above unity for the range of thicknesses investigated. It is worth noting that changing the probe forming semiangle to a large value does not bring the ratio closer to unity.

The local approximation for the effective ionization potential is assured for the EDX signal and calculations within that model facilitate discussing the subtleties of what contributes to the signal. So we continue the discussion with reference to that case. We now try to understand the results in Fig. 4(b) by considering in detail, first, the contribution to the signal from elastically scattered electrons and, then, that from electrons which have undergone thermal scattering prior to ionizing an atom.

A. Contribution to the signal from elastically scattered electrons

The separation of the contribution to the EELS or EDX signal from elastically and thermally scattered electrons is possible because the thermally scattered electrons are incoherent with respect to those in the elastic channel. In addition, the contributions to the detected signal from different atoms are mutually incoherent. This means that we can analyze the contribution to the signal when the probe is positioned over a particular column from atoms in that column and atoms in surrounding columns. We refer to these as on-column and off-column contributions, respectively, in what follows. This provides us with insight into where the signals due to elastically scattered electrons and those electrons which have been thermally scattered before ionization are generated in the specimen. In this subsection we consider the former contribution.

Figures 5(a) and 5(b) show the probe intensity, defined by the flux in the elastic channel, as a function of the depth in the specimen for the probe situated above the Ti/O and O

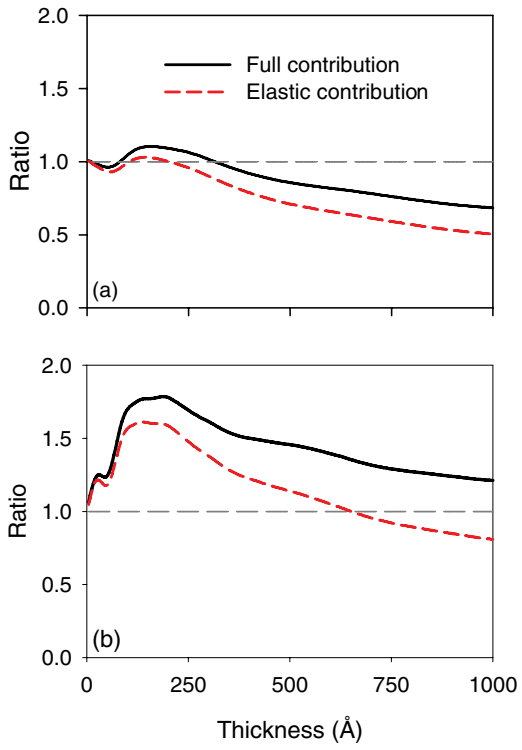

FIG. 4. (Color online) Ratio of the total oxygen signals on the Ti/O and the O columns as a function of thickness and of the contributions to the signal from elastically scattered electrons only as a function of thickness for (a) the EELS and (b) the EDX case (imaging parameters as specified in Sec. II). Based only on the density of atoms in the Ti/O and O columns, one would expect the ratio to be unity in each case.

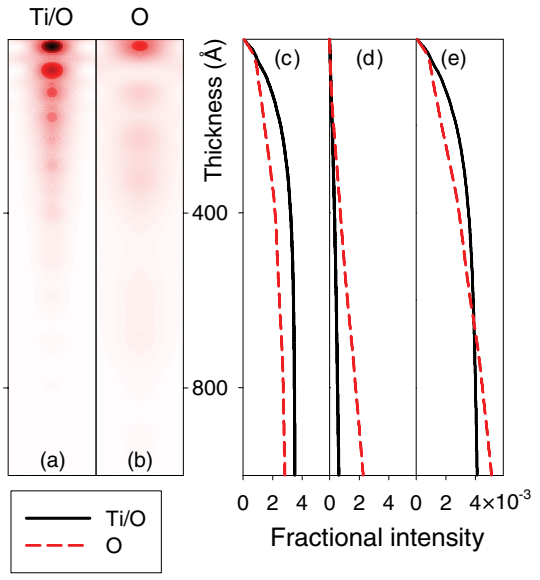

FIG. 5. (Color online) Calculations of the elastic probe profile in ⟨001⟩ strontium titanate with the probe on (a) a Ti/O column and (b) a pure O column. Cumulative plots are shown for the EDX signal for the O K shell from atoms (c) in the column under the probe and (d) in all other columns. (e) The sum of those contributions is plotted. Simulation parameters are as detailed for the EDX experiment in Sec. II.

columns. To obtain a sense of scale, the first "lobe" in the probe profile with the probe atop the Ti/O column in Fig. 5(a) encompasses approximately 12 titanium atoms in the vertical direction. These profiles are calculated by taking a 1-Å-long line trace through the probe intensity along the [100] direction. Figures 5(c)–5(e) are cumulative plots of the component of the EDX signal due to elastically scattered electrons, with Fig. 5(c) showing the on-column contributions, Fig. 5(d) showing the off-column contributions, and Fig. 5(e) indicating the total contribution from all atoms.

In Figs. 5(a) and 5(b), the *Pendellösung* effect seen when the probe is on the Ti/O column is less pronounced on the pure O column, due to the lower average atomic number of that column. On that column the probe is not strongly attracted to the column and hence is not strongly channeled. The intensity when on the Ti/O column is depleted at larger thicknesses due to thermal scattering by the titanium atoms.

A number of aspects should be noted here. First, for this range of thicknesses, the Ti/O column always has a higher on-column contribution. This is what one might expect based on the probe profiles shown. If one plots the derivatives of the curves shown in Fig. 5(c) (not shown here), then the maxima coincide with the lobes in the profiles, indicating that *Pendellösung* plays an important role in the strength of this contribution. Second, the off-column contribution is consistently higher on the pure oxygen column than on the Ti/O column. This can again be understood by examining the probe profiles. The probe, when positioned over the pure O column, is able to diffuse away from the column and interact with oxygen atoms in surrounding columns. In contrast, the probe is held more tightly on the Ti/O column and thus the off-column contribution is lower. Third, these two tendencies (larger on-column contributions on Ti/O columns due to stronger binding of the probe and larger off-column contributions on pure oxygen due to diffusion of the probe) are at odds with one another, and it is not obvious which should win out over the other. For lower thicknesses one might expect the binding tendency, and thus the Ti/O signal, to dominate, since the probe intensity is already situated around atoms where the ionization potential is peaked, whereas diffusion to neighboring O atoms will not occur immediately. Indeed this is the case. For thicknesses up to 600 Å, the total signal in Fig. 5(e) is higher for the probe positioned over a Ti/O column. However, for thicknesses larger than 600 Å the diffusion tendency wins out, and the total signal is higher for the probe positioned over pure oxygen.

At this point we make some more general statements. It appears that the presence of an element of high nuclear charge acts to increase the on-column contribution for elastically scattered electrons. However, such elements may also cause significant thermal scattering, depleting the signal and causing the on-column contribution to saturate. In simple terms, a column with a low average atomic number appears to allow the probe to diffuse away, resulting in a lower on-column contribution but increasing the off-column contribution. As a means of testing these statements, in a later section we perform similar calculations for the [110] direction in strontium titanate. This orientation also has both pure O columns and Sr/O columns with a higher average atomic number than the Ti/O columns.

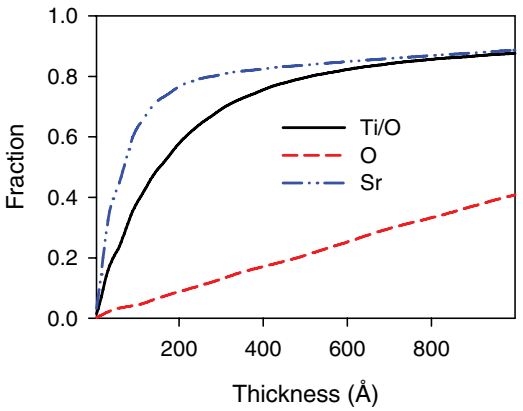

FIG. 6. (Color online) Fraction of the probe that has been thermally scattered at a given thickness, for probe positions above three different columns of atoms, as indicated, in ⟨001⟩ strontium titanate. Microscope parameters are those for EDX specified in Sec. II.

This section has looked only at the contributions to the signal due to ionization by elastically scattered electrons. As shown in Figs. 3(c) and 3(f), the thermal contribution is also important and, in fact, can cause a change in the total relative peak heights compared with the contribution to the signal from elastically scattered electrons. This contribution is studied in the following section.

B. Contribution to the signal from thermally scattered electrons

The extent to which thermal scattering might contribute to the spectroscopic signal can initially be gauged by examining the fraction of the probe that has been thermally scattered as a function of thickness for various probe positions. This is illustrated in Fig. 6, calculated for the EDX parameters given in Sec. II (briefly, a 23-mrad convergence semiangle electron probe at 200 kV). It is clear that there is a greater potential for ionization by thermally scattered electrons when the probe is on a Ti/O column than when it is on a pure O column, simply because more thermally scattered electrons are generated. The rapid increase in the fraction of electrons that have been thermally scattered (through large angles) when the probe is on a column of Sr is consistent with the fact that there is a significant contribution to the O K-shell signal, despite the lack of O atoms in the Sr column—as can be seen for either EELS or EDX in Figs. 3(c) and 3(f).

The thermal contribution to the EDX signal is plotted as a function of thickness alongside the elastic and total contributions in Fig. 7. As shown in Fig. 7(b), the contribution from thermally scattered electrons is much greater when the probe is on a Ti/O column than a pure O column. This, coupled with the contribution for elastic scattering in Fig. 7(a) [a repeat of Fig. 5(a), for ease of comparison], leads to the total signal being consistently larger when the probe is on Ti/O columns as opposed to pure O columns, as shown in Fig. 7(c).

In the previous section, the elastic contributions were divided into on-column and off-column contributions. For the case when the probe is positioned over the Ti/O column, only 14% of the elastic contributions over the 700-Å thickness were off-column. In contrast, here 77% of the contributions from thermally scattered electrons are off-column. Of the total

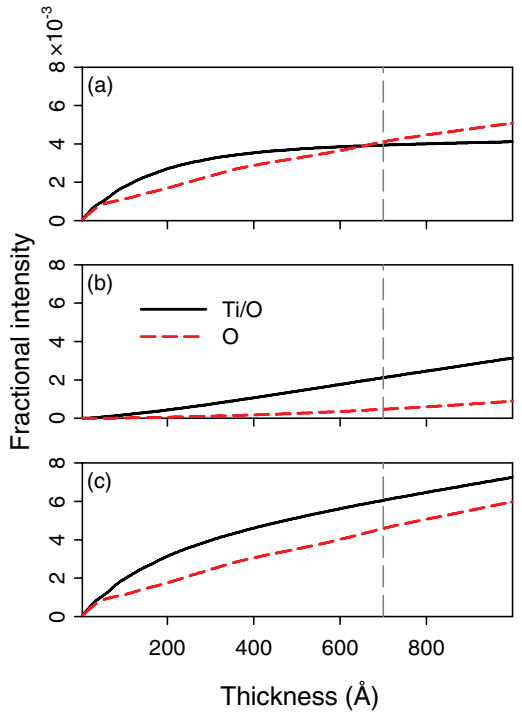

FIG. 7. (Color online) Contributions to the EDX oxygen K-shell signal in ⟨001⟩ strontium titanate due to (a) elastically scattered electrons, (b) thermally scattered electrons, and (c) all scattered electrons. Calculations were performed for the parameters given in Sec. II. The estimated thickness of the specimen is indicated (700 Å). (a) This is the same result as in Fig. 5 (e), repeated here for ease of comparison.

signal recorded for the Ti/O probe position, 33% is contributed by off-column ionization events. The origin of this effect is the large spatial area covered by the thermally scattered electrons (due to the characteristic high-angle scattering).

Figure 8 shows the depth-integrated *real-space* distribution of thermally scattered electrons, with the probe positioned over the Ti/O column. The specimen structure is overlaid, and a logarithmic transformation $x \rightarrow \log(1 + Cx)$, where x is the pixel value and $C = 10^4$, has been applied to the data to highlight interesting features. Prominent radial lines can be seen, and inspection of the overlaid specimen structure shows that the lines correspond to closely spaced collinear heavy atoms, i.e., those that cause significant thermal scattering. In loose terms, these can be thought of as a real-space analogy of the Kikuchi lines often seen in diffraction patterns.

These radial lines of thermally scattered intensity extend far from the column lying below the probe. As shown in Eq. (4), wherever the intensity overlaps with the ionization potential there will be a contribution to the signal. This confirms that there will be significant contributions from those oxygen atoms lying along the "thermal rays." These contributions reduce the extent to which the calculated elemental map represents localized information about the specimen structure. The relative peak height recorded for different probe positions also reflects structure-containing information from surrounding columns, especially for larger thicknesses ($\gtrsim$200 Å for the case studied here).

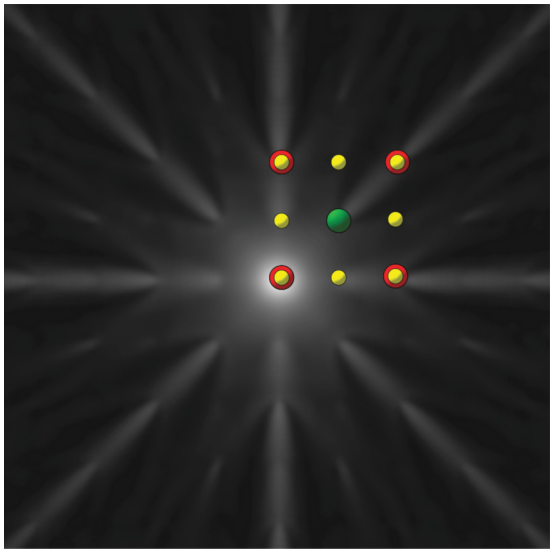

FIG. 8. (Color online) Depth-integrated *real-space* distribution of thermally scattered electrons for a thickness of 700 Å with the probe positioned over a Ti/O column in ⟨001⟩ strontium titanate. The specimen structure is overlaid. A logarithmic transformation $x \rightarrow \log(1 + Cx)$, where x is the pixel value and $C = 10^4$, has been applied to the calculated results to highlight interesting features.

C. Different crystal orientation

Let us now consider ⟨110⟩ strontium titanate as a contrast to the results discussed in Secs. IV A and IV B. In Fig. 9 we show an EDX elemental map for the oxygen K edge in ⟨110⟩ strontium titanate, Fig. 9(a) showing the raw data and Fig. 9(b) a filtered average using a 9 × 9-pixel moving-average square window. An intensity profile along the line drawn in Fig. 9(b) is shown in Fig. 9(c), and from this figure, we note that the signal on the pure O columns is greater than that on the Sr/O columns. While it is recognized that this profile is not an absolute measure of intensity (because of the averaging technique), this result is not unexpected since the linear density of oxygen atoms in the pure O columns is twice that in the Sr/O columns. Close inspection of the ratio of signals on the two kinds of oxygen columns shows that the ratio is slightly greater than 2, as shown in Fig. 9(c). However, this is fortuitous and our simulations in Fig. 10, discussed in the next paragraph, show that this is not true for all specimen thicknesses.

As we did in Sec. IV (see Fig. 4), let us investigate how the signals on the Sr/O and the pure O columns compare as a function of thickness. In Fig. 10 we have plotted the ratio of the total signal when the probe is on Sr/O columns to that on pure O columns as a function of thickness. The ratio is also shown for the contribution from elastically scattered electrons only. It is shown that the ratio generally varies from the value of one-half that one might expect in view of the fact that the density of oxygen in the Sr/O columns is half that in the pure O columns. As before, we now try to understand this by considering in detail, first, the contribution to the signal from elastically scattered electrons and that from electrons which have undergone thermal scattering prior to ionizing an atom.

In Fig. 11 we show calculations equivalent to those in Fig. 5 for the [001] orientation. As before, the Sr/O column elicits strong *Pendellösung*, due to the high average atomic number.

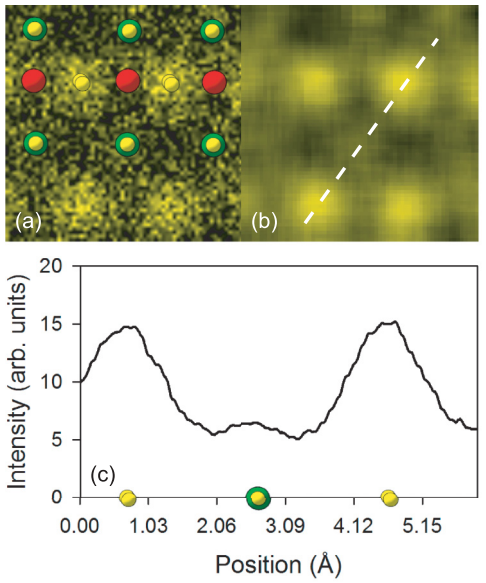

FIG. 9. (Color online) (a) An EDX elemental map of ⟨110⟩ strontium titanate monitoring the oxygen K edge for a single scan (raw data). (b) Result of applying a 9×9-pixel moving-average square window to the original data. (c) A scan across Sr/O and O columns as indicated in (b) (and which had a width of 8 pixels). The projected structure and, in particular, the positions of the Sr/O [large (green) rings and small inset (yellow) circles] and O columns [small (yellow) circles] are indicated. The large solid (red) circles in (a) indicate the position of the Ti columns. Experimental parameters are similar to those specified in Sec. II for the data in Fig. 2.

Furthermore, there is strong depletion of the probe on an Sr/O column due to thermal scattering, which is markedly greater in this case than for the Ti/O column previously. When the probe is above a pure oxygen column it is attracted more strongly to the column, with less diffusion away. This difference is quite marked given that the linear oxygen density only increases by a factor of 1.4 in this orientation relative to the [001] case. These differences manifest themselves as qualitative differences

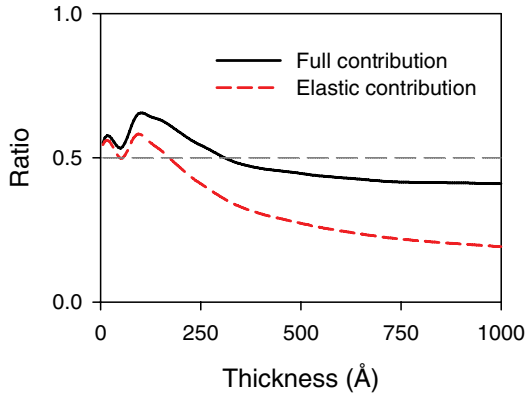

FIG. 10. (Color online) Ratio of the total oxygen signals on Sr/O and O columns as a function of the thickness and of the contributions to the signal from elastically scattered electrons only as a function of thickness for the EDX case (imaging parameters as specified in Sec. II). Based only on the density of atoms in the Sr/O and O columns, one would naively expect the ratio to be one-half.

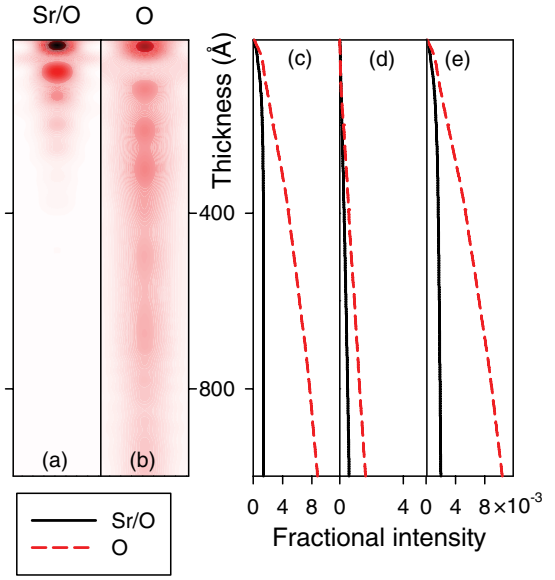

FIG. 11. (Color online) Calculations of the elastic probe profile in ⟨110⟩ strontium titanate with the probe on (a) a Sr/O column and (b) a pure O column. Cumulative plots are shown for the EDX signal for the O K shell from atoms (c) in the column under the probe and (d) in all other columns. (e) The sum of those contributions is plotted. Simulation parameters are as detailed for the EDX experiment in Sec. II.

between the elastic signal contributions in Figs. 11(c)–11(e) and those for the [001] orientation in Figs. 5(c)–5(e). The on-column contribution from elastically scattered electrons

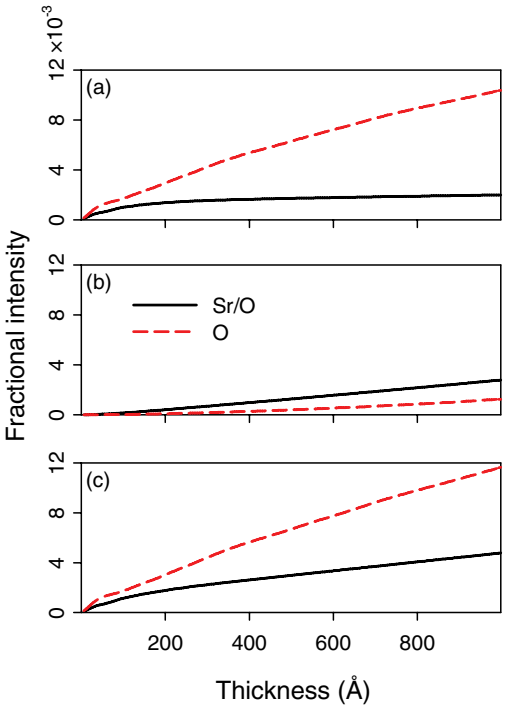

FIG. 12. (Color online) Contributions to the EDX oxygen K-shell signal in ⟨110⟩ strontium titanate due to (a) elastically scattered, (b) thermally scattered, and (c) all scattered electrons. Calculations were performed for the parameters given in Sec. II. (a) This is the same result as in Fig. 11(e), repeated here for ease of comparison.

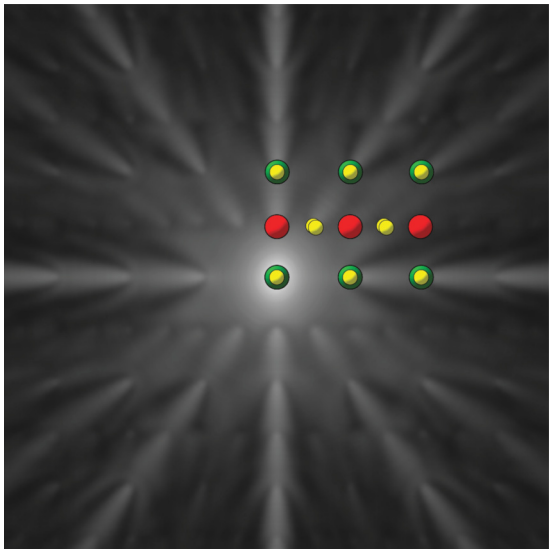

FIG. 13. (Color online) Depth-integrated *real-space* distribution of thermally scattered electrons for a thickness of 700 Å with the probe positioned over the Sr/O column in ⟨110⟩ strontium titanate. The specimen structure is overlaid. A logarithmic transformation $x \rightarrow \log(1 + Cx)$, where x is the pixel value and $C = 10^4$, has been applied to the calculated results to highlight interesting features.

when the probe is above the Sr/O column is now consistently much less than the on-column contribution when the probe is on the pure O column. Even considering the fact that the latter has twice the oxygen density of the former, this is a significant qualitative change. This results from features discussed above: Sr causes more thermal scattering than Ti, leading to a reduced probe flux on the column and hence a reduced on-column contribution. Furthermore, the increased linear density of oxygen in the pure O columns holds the probe to the columns more effectively, leading to an increased on-column contribution. In this case the off-column elastic contributions are negligible, since on both columns the probe does not get a chance to diffuse away from the probe position.

In Fig. 12 we present calculations equivalent to those for the [001] orientation presented in Fig. 7. Figure 12(a) is a reprise of the total elastic contribution shown in Fig. 11(e). In Fig. 12(b) we see that, by comparison with Fig. 7(b), the contribution from thermally scattered electrons is reduced, despite the fact that there is more thermal scattering on the Sr/O column than on the Ti/O. This is due to the way in which these thermally scattered electrons interact with the surrounding specimen structure. To be more specific, for a Ti/O column there is a higher linear density of oxygen atoms and nearby oxygen atoms are closer to the column, where the flux of thermally scattered electrons is higher. A representation of this interaction is shown in Fig. 13, which can be compared with Fig. 8. There are two things to note here. First, there is an enhanced contribution from elastic scattering on the pure oxygen columns, due to the tighter binding of the probe to those columns. Second, there is a reduced contribution due to elastic scattering on the Sr/O columns, due to the probe being depleted by thermal scattering. Hence, the role played by the thermal contribution in Fig. 12(b) is different in this case.

V. CONCLUSION

We have presented apparently anomalous results observed in EELS and EDX elemental maps of the oxygen K-shell edge in ⟨001⟩ strontium titanate. The relative peak heights observed were not consistent with the fact that the density of oxygen in the mixed Ti/O and pure O columns is the same, but, perhaps contrary to expectations, the larger signal was on the Ti/O columns. Using the recently developed model for the elastic and thermal scattering of fast electrons in a specimen based on a BO approximation, we calculated the contribution to the oxygen K-shell signal from elastically scattered electrons and those which had been thermally scattered (possibly multiple times). It was the latter component which was responsible for the larger signal on the Ti/O column. One can additionally analyze from which atomic columns the elastic and thermal contributions arise. In particular, this shows that the contribution to the signal from thermally scattered electrons is quite delocalized in the sense that there is a considerable contribution from oxygen atoms in columns other than that on which the probe is positioned and at a considerable distance away. We compared these results to an analysis of data for ⟨110⟩ strontium titanate. The results in this paper underline the crucial role that simulations play in the interpretation of atomic resolution elemental mapping. Experiments *in tandem with* the theoretical models described in this paper can provide a plausible interpretation of the structure at the atomic level.

ACKNOWLEDGMENTS

This research was supported under the Discovery Projects funding scheme of the Australian Research Council (Project No. DP110102228) and by the Center for Emergent Materials at the Ohio State University, an NSF MRSEC (Award No. DMR-0820414).

*Corresponding author: lja@unimelb.edu.au

[1]M. Bosman, V. J. Keast, J. L. García-Muñoz, A. J. D'Alfonso, S. D. Findlay, and L. J. Allen, Phys. Rev. Lett. **99**, 086102 (2007).

[2]K. Kimoto, T. Asaka, T. Nagai, M. Saito, Y. Matsui, and K. Ishizuka, Nature **450**, 702 (2007).

[3]D. A. Muller, L. Fitting Kourkoutis, M. Murfitt, J. H. Song, H. Y. Hwang, J. Silcox, N. Dellby, and O. L. Krivanek, Science **319**, 1073 (2008).

[4]L. J. Allen, Nature Nanotechnol. **3**, 255 (2008).

[5]S. Trasobares, M. López-Haro, M. Kociak, K. March, F. de La Peña, J. A. Perez-Omil, J. J. Calvino, N. R. Lugg, A. J. D'Alfonso, L. J. Allen *et al.*, Angew. Chem. Int. Ed. **50**, 868 (2011).

[6]A. J. D'Alfonso, B. Freitag, D. Klenov, and L. J. Allen, Phys. Rev. B **81**, 100101(R) (2010).

[7]M. W. Chu, S. C. Liou, C. P. Chang, F. S. Choa, and C. H. Chen, Phys. Rev. Lett. **104**, 196101 (2010).

[8]L. J. Allen, A. J. D'Alfonso, B. Freitag, and D. O. Klenov, MRS Bull. **37**, 47 (2012).

[9]K. J. Dudeck, M. Couillard, S. Lazar, C. Dwyer, and G. A. Botton, Micron **43**, 57 (2012).
[10]P. Wang, A. J. D'Alfonso, S. D. Findlay, L. J. Allen, and A. L. Bleloch, Phys. Rev. Lett. **101**, 236102 (2008).
[11]B. D. Forbes, A. V. Martin, S. D. Findlay, A. J. D'Alfonso, and L. J. Allen, Phys. Rev. B **82**, 104103 (2010).
[12]R. F. Loane, P. Xu, and J. Silcox, Acta Crystallogr. Sec. A **47**, 267 (1991).
[13]E. J. Kirkland, *Advanced Computing in Electron Microscopy* (Plenum Press, New York, 1998).
[14]L. J. Allen, S. D. Findlay, M. P. Oxley, and C. J. Rossouw, Ultramicroscopy **96**, 47 (2003).
[15]S. D. Findlay, L. J. Allen, M. P. Oxley, and C. J. Rossouw, Ultramicroscopy **96**, 65 (2003).
[16]S. D. Findlay, M. P. Oxley, S. J. Pennycook, and L. J. Allen, Ultramicroscopy **104**, 126 (2005).
[17]C. R. Hall and P. B. Hirsch, Proc. R. Soc. London A **286**, 158 (1965).
[18]C. J. Rossouw, C. T. Forwood, M. A. Gibson, and P. R. Miller, Micron **28**, 125 (1997).